AMERICAN SOCIETY FOR MICROBIOLOGY | Journal of Virology

Type I Interferon Response Limits Astrovirus Replication and Protects against Increased Barrier Permeability *In Vitro* and *In Vivo*

Shauna A. Marvin,[a] C. Theodore Huerta,[a,b]* Bridgett Sharp,[a] Pamela Freiden,[a] Troy D. Cline,[c] Stacey Schultz-Cherry[a]

Department of Infectious Diseases, St. Jude Children's Research Hospital, Memphis, Tennessee, USA[a]; Rhodes College, Memphis, Tennessee, USA[b]; Department of Biological Sciences, California State University, Chico, California, USA[c]

ABSTRACT

Little is known about intrinsic epithelial cell responses against astrovirus infection. Here we show that human astrovirus type 1 (HAstV-1) infection induces type I interferon (beta interferon [IFN-β]) production in differentiated Caco2 cells, which not only inhibits viral replication by blocking positive-strand viral RNA and capsid protein synthesis but also protects against HAstV-1-increased barrier permeability. Excitingly, we found similar results *in vivo* using a murine astrovirus (MuAstV) model, providing new evidence that virus-induced type I IFNs may protect against astrovirus replication and pathogenesis *in vivo*.

IMPORTANCE

Human astroviruses are a major cause of pediatric diarrhea, yet little is known about the immune response. Here we show that type I interferon limits astrovirus infection and preserves barrier permeability both *in vitro* and *in vivo*. Importantly, we characterized a new mouse model for studying astrovirus replication and pathogenesis.

The successful replication and spread of many enteric viruses depend upon modulating immune factors produced by intestinal epithelial cells (IECs) including interferons (IFNs) (1, 2). For instance, enteric adenoviruses are sensitive to IEC-produced type I IFNs, unlike respiratory adenoviruses (3), while rotavirus exploits type I IFN signaling in IECs to promote early viral replication (4). However, nothing is known about the impact of IFN on astrovirus infection.

Astroviruses are small, nonenveloped, RNA viruses that are one of the most important causes of pediatric acute gastroenteritis worldwide (5–8). Infection begins by binding to an unidentified receptor(s) on epithelial cells after fecal-oral transmission followed by entry via endosomes (9). After viral uncoating, the positive-sense, single-stranded RNA genome is translated into a polyprotein precursor that is subsequently cleaved into proteins required for replication and the assembly of progeny virions. The genome contains three open reading frames: ORF1a, ORF1b, and ORF2. ORF1a and ORF1b encode nonstructural proteins involved in transcription and replication of the virus, while ORF2 encodes the capsid protein (10, 11). Negative-strand RNA is produced from the positive genomic strand, which can be detected 6 to 12 h postinfection (hpi) (12). Transcription of the negative-strand genome yields the genomic and subgenomic RNA. Human astrovirus (HAstV) proteins have been associated with membranes in infected cells likely serving as the site for replication and assembly (13–15). After assembly, the progeny virions egress from the cell, a process promoted by caspase activation (16).

Recently, Guix et al. found that HAstV type 4 (HAstV-4) replication induces type I IFN production and that pretreatment of Caco2 cells with beta interferon (IFN-β) reduced HAstV-4 capsid protein synthesis and progeny virion production (17). However, whether the IFN-β produced during astrovirus infection is sufficient to limit astrovirus replication, and at what step in the viral life cycle IFN-β affects astrovirus, remains unknown. Additionally, whether IFN-β has an impact on astrovirus pathogenesis has not been determined.

In these studies, we demonstrate that HAstV-1 replication in differentiated Caco2 cells also induces type I IFN, which can then limit viral replication in a dose-dependent manner. Neutralization of virus-induced IFN-β leads to higher viral titers *in vitro*, highlighting the importance in limiting viral spread. Previously, we revealed that astrovirus infection increased the permeability of differentiated Caco2 cells as measured by a drop in transepithelial resistance (TER) and increased flux of fluorescein isothiocyanate (FITC)-dextran from the apical side to the basolateral side of the polarized monolayer independent of cell death (18). However, this increased permeability was transient with the monolayer beginning to recover within 48 to 72 hpi. Our current studies may partially explain this finding by demonstrating the importance of astrovirus-induced type I IFN in protecting the intestinal epithelium from increased barrier permeability.

To begin defining the role of type I IFN *in vivo*, we developed a new animal model of astrovirus pathogenesis. To date, young turkeys (poults) infected with turkey astrovirus type 2 (TAstV-2) are the best defined animal model for astrovirus pathogenesis (19). Unfortunately, the lack of reagents, laboratory facilities, and expertise with the species, as well as availability of birds, severely limits this model. Here we not only describe a new murine astrovirus (MuAstV) model but also highlight the important role for

Received 15 September 2015 **Accepted** 30 November 2015

Accepted manuscript posted online 9 December 2015

Citation Marvin SA, Huerta CT, Sharp B, Freiden P, Cline TD, Schultz-Cherry S. 2016. Type I interferon response limits astrovirus replication and protects against increased barrier permeability *in vitro* and *in vivo*. J Virol 90:1988–1996. doi:10.1128/JVI.02367-15.

Editor: T. S. Dermody

Address correspondence to Troy D. Cline, tdcline@csuchico.edu, or Stacey Schultz-Cherry, stacey.schultz-cherry@stjude.org.

* Present address: C. Theodore Huerta, University of Kentucky College of Medicine, Lexington, Kentucky, USA.

S.A.M. and C.T.H. contributed equally to this work.

type I IFN in limiting viral replication and potentially protecting against astrovirus-increased barrier permeability *in vivo*.

MATERIALS AND METHODS

Cells. The human intestinal adenocarcinoma cell line Caco2 was obtained from ATCC (HTB-37). Cells were propagated in minimum essential medium (MEM; Corning) supplemented with 10% fetal bovine serum (FBS; Benchmark), glutaMax-I (Gibco), 1 mM sodium pyruvate (Gibco), and penicillin-streptomycin (Gibco). To differentiate Caco2 cells, the cells were plated on 1-μm-pore-size transwell inserts (Corning) at 5×10^4 cells/well and incubated for 3 or 4 days until the transepithelial electrical resistance (TER) measurements registered greater than 1,000 $\Omega \cdot cm^2$ and the cells formed a polarized monolayer as described previously (18).

Daoy cells were obtained from ATCC (HTB-186) and cultured in Eagle's minimum essential medium (Lonza) supplemented with 10% FBS, glutaMax-I, and nonessential amino acids (Gibco). All cells were cultured at 37°C with 5% CO_2.

Viruses. HAstV-1 was propagated in Caco2 cells, and the titers of the virus were determined on Caco2 cells by the fluorescent-focus assay (focus-forming units [FFU]) as previously described (20). Briefly, 2×10^4 cells were seeded into 96-well plates, and after 3 days, the cells were inoculated with 10-fold dilutions of HAstV-1 in MEM containing 0.3% bovine serum albumin (BSA) for 1 h at 37°C, at which time the virus was replaced with MEM containing 0.3% BSA. After 16 to 24 h, cells were fixed with 4% formaldehyde (Polysciences), permeabilized with 0.5% (vol/vol) Triton X-100 in phosphate-buffered saline (PBS) for 15 min, and then blocked with 10% FBS in PBS at room temperature. The cells were stained with HAstV monoclonal antibody 8E7 (2 μg/ml DakoCytomation) for 1 h at 37°C followed by anti-mouse IgG labeled with Alexa Fluor 488 (anti-mouse IgG-Alexa Fluor 488) (1:400) (Invitrogen) secondary antibodies and DAPI (4′,6′-diamidino-2-phenylindole) (Sigma) for 1 h at 37°C. Wells were imaged on an EVOS microscope (Advanced Microscopy Group) using identical parameters for each treatment. Nuclei and fluorescein isothiocyanate (FITC)-positive (FITC+) cells were counted using ImageJ software. The average FFU per milliliter was calculated as follows: (number of FITC+ cells/number of cells) multiplied by the average number of cells per well multiplied by the dilution factor. To UV inactivate the virus, 50 μl of HAstV-1 was subjected to 100 mJ/cm^2 with a UV cross-linker as described previously (18), and inactivation was confirmed by the fluorescent-focus assay.

The A/Puerto Rico/8/1934 influenza virus lacking the NS1 gene (PR8-ΔNS1) was provided by Adolfo Garcia-Sastre (Icahn School of Medicine, Mount Sinai) (21) and propagated in eggs, and virus titer in MDCK cells was determined by microneutralization assay as described previously (22). Vesicular stomatitis virus (VSV) was a kind gift from Michael Whitt, University of Tennessee Health Science Center, Memphis, TN.

MuAstV. Mouse colonies at St. Jude Children's Research Hospital were screened for the presence of murine astrovirus (MuAstV) by real-time reverse transcription-PCR (RT-PCR) as described previously (23). We identified several immunocompromised colonies persistently infected with MuAstV, including our IFNaR$^{-/-}$ (IFNaR stands for alpha interferon receptor) mice.

MuAstV stocks were prepared from feces collected from persistently MuAstV-infected mice. Briefly, for 12 tubes, 250 μl of feces was suspended in 0.5 ml PBS in each tube, homogenized using 2-mm zirconium oxide beads (Next Advance) beads for 4 min on speed setting 4 (Next Advance air cooling bullet blender), and pelleted by centrifugation at 12,000 rpm for 5 min. The supernatants were pooled and filtered through a 0.2-μm filter (fecal filtrate) and viral copy number quantified by real-time RT-PCR (23). Briefly, viral RNA was isolated from feces by the QIAamp viral RNA minikit (Qiagen) according to the manufacturer's instructions. cDNA was synthesized from 1 μg of total RNA using the SuperScript VILO cDNA synthesis kit (Invitrogen), and 2 μl was used for real-time RT-PCR. PCR was performed using AmpliTaq Gold 360 DNA polymerase reagents (Applied Biosciences) and forward primer 5′TACA TCGAGCGGGTGGTCGC, reverse primer 5′GTGTCACTAACGCGCA CCTTTTCA, and probe 6-carboxyfluorescein (6FAM)-TTTGGCATGTG GGTTAA-MBGNFQ (minor groove binder nonfluorescent quencher) under the following conditions: 95°C for 10 min, followed by 50 cycles, with 1 cycle consisting of 95°C for 15 s and 60°C for 1 min on a Bio-Rad CFX96 real-time PCR detection system. The number of genome copies/microgram of total RNA was determined using the threshold cycle (C_T) value of the sample compared to a standard curve generated from a synthesized MuAstV DNA from nucleotides 3819 to 4279 with a known copy number (calculated using Thermo Fisher Scientific DNA Copy Number and Dilution Calculator [www.thermofisher.com]). Log_{10} dilutions of the synthesized MuAstV DNA were used for real-time RT-PCR as described above. C_T values versus nanogram of DNA were plotted, and the equation, which included the *y*-axis intercept and slope, were calculated using Microsoft Excel to generate the standard curve. C_T values from experimental samples were converted into copy number using the calculated standard curve, multiplied by the dilution factor of cDNA used, multiplied by the number of genome copies per microgram of total RNA.

The ORF2 region of MuAstV from mice within our colony was sequenced using Qiagen one-step RT-PCR (catalog no. 210212) with Invitrogen RNaseOut (catalog no. 10777-019) and forward primer 5′CCACC ACCYGAGTCYGGACCCTA and reverse primer 5′TGGTTRCGGTAGG GCCAGCGRTT under the following conditions: 50°C for 50 min, 95°C for 15 min, followed by 30 cycles, with 1 cycle consisting of 95°C for 30 s, 50°C for 30 s, and 68°C for 45 s, followed by a final elongation step of 68°C for 5 min. Sequences were obtained by the St. Jude Hartwell Center and aligned using BioEdit and MEGA6.

Type I IFN treatments and reagents. Differentiated Caco2 cells in transwell plates were washed once with PBS, incubated in serum-free medium, and then inoculated with HAstV-1 (at a multiplicity of infection [MOI] of 1 unless otherwise indicated) for 1 h. Cells were then washed and incubated for 16 to 24 hpi. For experiments that included exogenous IFN-β treatment, cells were pretreated overnight and infected in the presence of 1 μg/ml of IFN-β (Preprotech). For experiments that included neutralizing IFN-β, cells were infected in the presence of 3 μg/ml anti-IFN-β antibody (Abcam) or isotype control IgG.

Quantitating HAstV-1 positive- and negative-strand synthesis. Positive- and negative-strand RNA was quantitated by semiquantitative reverse transcription-PCR as described previously (24). Briefly, cells were collected at the indicated time point in TRIzol reagent (Thermo Fisher Scientific) and RNA was isolated according to the manufacturer's instructions. RT reactions on 1 μg total RNA were performed using SuperScript III first-strand synthesis system (catalog no. 18080-51; Invitrogen) and 0.5 μM primer, Mon348 (for positive strand) or Mon344 (for negative strand) primers (25), according to the manufacturer's instructions. RT reactions for β-actin were performed using the SuperScript VILO cDNA synthesis kit (Invitrogen) according to the manufacturer's instructions. PCR mixtures were composed of *Taq* DNA polymerase enzyme and buffers (Qiagen) using 2 μl of cDNA. Primer pairs included Mon340 and Mon348 (positive strand), Mon343 and Mon344 (negative strand) (25), or β-actin (forward primer 5′GCTGTGCTATCCCTGTA and reverse primer 5′GCCTCAGGGCAGCGG). PCR was performed as follows: 94°C for 2 min, 30 cycles, with 1 cycle consisting of 94°C for 30 s, 54°C for 30 s, and 72°C for 3 min, with a final extension cycle of 72°C for 10 min. PCR products (5 μl) were separated on 2% agarose gels and visualized on a FOTODYNE UV-transilluminator using FOTO/Analyst PC Image software. Band intensities were compared using ImageJ software.

Recombinant HAstV-1 capsid protein production and purification. Recombinant HAstV-1 capsid protein was expressed in Sf9 cells and purified by HisTrap metal affinity chromatography by the St. Jude Children's Research Hospital Protein Production Facility as described previously (18, 26, 27). Protein concentrations were quantified by the bicinchoninic acid (BCA) protein assay kit (Pierce), and purification was confirmed by SDS-PAGE.

Determining IFN levels. Type I IFN mRNA levels were determined as described previously (28). Briefly, Caco2 or Daoy cells were plated at 5×10^4 cells in 24-well tissue culture plates or 24-well tissue culture transwells, respectively, and incubated for 2 or 3 days until confluent (culture plate) or until the TER reached 1,000 $\Omega \cdot cm^2$ (transwells) as described above. The cells were then inoculated with PBS alone (mock infected), HAstV-1 (MOI of 1), UV-inactivated HAstV-1, purified HAstV-1 capsid (5 μg) or influenza PR8-ΔNS1 (MOI of 0.3), and cell supernatants or lysates were collected at different times postinfection. RNA was isolated from cells by TRIzol extraction according to the manufacturer's instructions. To determine IFN-β RNA levels, 100 ng of RNA was screened via TaqMan Fast Virus one-step master mix and IFN-β forward primer 5′CGCCGCATTG ACCATCTA, reverse primer 5′GACATTAGCCAGGAGCTTCTCA, and probe 5′ 6-FAM-TCAGACAAGATTCATCTA by real-time PCR on a Bio-Rad CFX96 real-time PCR detection system. Human glyceraldehyde-3-phosphate dehydrogenase (GAPDH) control reagents (TaqMan [catalog no. 402869; Life Technologies]) were included in the reaction mixtures as a loading control (0.4 μl each of forward primer, reverse primer, and probe). PCRs were as follows: 50°C for 50 min, 95°C for 20 s, followed by 45 cycles, with 1 cycle consisting of 95°C for 3 s and 60°C for 30 s. The amount of IFN-β was normalized to GAPDH. Results are shown as fold increase over mock-infected cells at the same time point.

To quantitate type I IFN protein levels, a VSV bioassay was performed as described previously (29). Briefly, Daoy cells were plated at 2.5×10^4 per well in a 96-well tissue culture plate, incubated overnight, and then infected with 2-fold serial dilutions of supernatants collected from Caco2 cells 24 h after HAstV-1 (MOI of 1) or PR8 (MOI of 0.3) infection. Supernatants were acid treated with an equal volume of MEM containing 0.1 N HCl for 2 h at room temperature and then neutralized with 7.5% $NaHCO_3$ to inactivate IFN-γ prior to addition to Daoy cells. Increasing concentrations of human IFN-β from 0 to 500 pg/ml served as the positive control. Twenty-four hours later, cells were inoculated with 1×10^5 PFU of VSV and incubated for 2 days. The medium was removed, and cells were stained with crystal violet at room temperature for 30 min. The amount of IFN was calculated by multiplying the dilution of supernatant that gave 50% protection for the cytopathic effect (CPE) by the standard amount of IFN-β that gave 50% protection for CPE.

Animal experiments. All procedures were approved by the St. Jude Children's Research Hospital Institutional Animal Care and Use Committee and were in compliance with the *Guide for the Care and Use of Laboratory Animals* (30). Stool samples from 3- to 6-week-old male and female wild-type (WT) C57BL/6 mice (Jackson Laboratories) and $IFNaR^{-/-}$ mice (St. Jude Children's Research Hospital colony) were prescreened for MuAstV by real-time RT-PCR as described above. WT mice were shown to be negative for MuAstV, while all $IFNaR^{-/-}$ mice in our colony were MuAstV positive. Regardless, mice were orally gavaged with a fecal filtrate containing 2×10^7 MuAstV in 100 μl PBS or PBS alone. Viral shedding was monitored by obtaining fresh feces (approximately 50 mg) from individual mice every 48 to 72 h and analyzed by real-time RT-PCR and converted into copy number per 1 μg RNA as described above. After 21 days postinfection (dpi), feces were collected and screened at days 39 and 53 postinfection.

Measuring barrier permeability. We used two assays to monitor the permeability of epithelial, transepithelial electrical resistance and fluorescent flux. TER measures ion movement across a barrier and is an indirect measurement of tight junctions (31). Fluorescent flux directly measures the paracellular permeability of an inert dye from the apical side of the cell monolayer to the basolateral side (18). Caco2 cells were plated at 5×10^4 cells/well on 0.3-cm^2 semipermeable tissue culture inserts (Corning) and incubated for 3 or 4 days until the TER reached 1,000 $\Omega \cdot cm^2$. Cells were then apically infected with HAstV-1 (MOI of 2) in the presence or absence of IFN-β (1 μg/ml), and TER levels were measured at the indicated time points using an EndOhm-6 chamber and $EVOM^2$ epithelial voltohmmeter (World Precision Instruments). Results are presented as percentages of the insert's initial TER reading (time zero). Fluorescent flux of 20-kDa FITC-dextran (Sigma-Aldrich) was monitored *in vitro* as described previously (18). Briefly, differentiated Caco2 cells on transwell inserts were infected with HAstV-1 (MOI of 2) in the presence or absence of IFN-β (1 μg/ml), anti-IFN neutralizing antibody (3 μg/ml), or isotype control antibody. After 1 h, virus was removed and replaced with 100 μl of medium with a 1:50 dilution of 20-kDa FITC-dextran (20 mg/ml) to the apical surface in the presence or absence of IFN-β, anti-IFN neutralizing antibody, or isotype control antibody. At 24, 48, and 72 hpi, 50 μl of supernatant from the basolateral chamber was collected, and fluorescence was measured on a Fluoroskan Ascent fluorometer (Thermo Labsystems) at an excitation wavelength of 435 nm and an emission wavelength of 538 nm. Fluorescence was compared to that of maximum migration of the FITC-dextran probe across a cell-free insert, and results are expressed as percentage of the maximum migration (percentage of no cells).

Intestinal permeability *in vivo* was measured as previously described (32). Briefly, mice were orally gavaged with 10 mg/100 g of body weight 4-kDa FITC-dextran in 100 μl at 3 dpi. Four hours postinoculation, blood samples were collected retro-orbitally, and serum samples were isolated after 2 h at room temperature by centrifugation at 3,500 rpm at 4°C for 20 min. FITC in 25 μl sera was measured at an excitation wavelength of 485 nm and an emission wavelength of 538 nm. The amount of FITC-dextran in the serum was quantified by comparison to a FITC-dextran standard curve of the original inoculum stock.

Statistical analysis. The statistical significance of the data was determined by using the two-tailed Student *t* test in Microsoft Excel. Data are representative of or the average of at least two independent experiments run with at least duplicate samples. Mouse studies included 8 mice for PBS-inoculated mice and 12 or 13 mice per strain for MuAstV-inoculated mice. Error bars represent standard deviation, and statistical significance was defined as a P value of <0.05.

RESULTS

HAstV-1 induces IFN-β production. To determine whether IFN-β levels increased during HAstV-1 infection, differentiated Caco2 cells were infected with HAstV-1 (MOI of 1). NS1-deleted A/Puerto Rico/8/34 (PR8-ΔNS1) H1N1 influenza virus (MOI of 0.3), which is unable to disrupt IFN synthesis (33–36), was used as a control. Cells were collected at the time points indicated in the figures, and IFN-β mRNA levels were determined by real-time RT-PCR. HAstV-1 infection increased IFN-β expression in differentiated Caco2 cells 3-fold at 24 h postinfection (hpi) compared to mock-infected cells (Fig. 1A). HAstV-1 induction of IFN-β production requires viral replication, as UV-inactivated virus or HAstV-1 capsid protein, which assembles into virus-like particles (18) did not induce IFN-β expression (Fig. 1B). In contrast, ΔNS1 influenza virus increased production within 6 hpi, culminating in a 12-fold increase in IFN-β mRNA at 24 hpi (Fig. 1A).

To calculate the level of type I IFN activity induced by infection, a functional IFN bioassay was performed on cell supernatants from HAstV-1-infected and PR8-ΔNS1-infected cells collected at 24 hpi. Supernatants were acid treated to destroy IFN-γ, applied to Daoy cells, and subsequently challenged with vesicular stomatitis virus (VSV) as described previously (29). HAstV-1 induced a significantly higher level of type I IFN activity compared to mock-infected cells, although at a much lower level than ΔNS1 influenza virus (136.5 pg/ml versus 965 pg/ml [Fig. 1C]). Importantly, Daoy cells do not support HAstV-1 replication (Fig. 1D), and IFN-β RNA levels are not induced in Daoy cells directly inoculated with HAstV-1 or PR8-ΔNS1 influenza virus (Fig. 1E), demonstrating that the type I IFN measured in the bioassay is produced from the primary infection of Caco2 cells and not from any virus in the cell supernatants.

IFN-β limits HAstV-1 replication. Having established the ki-

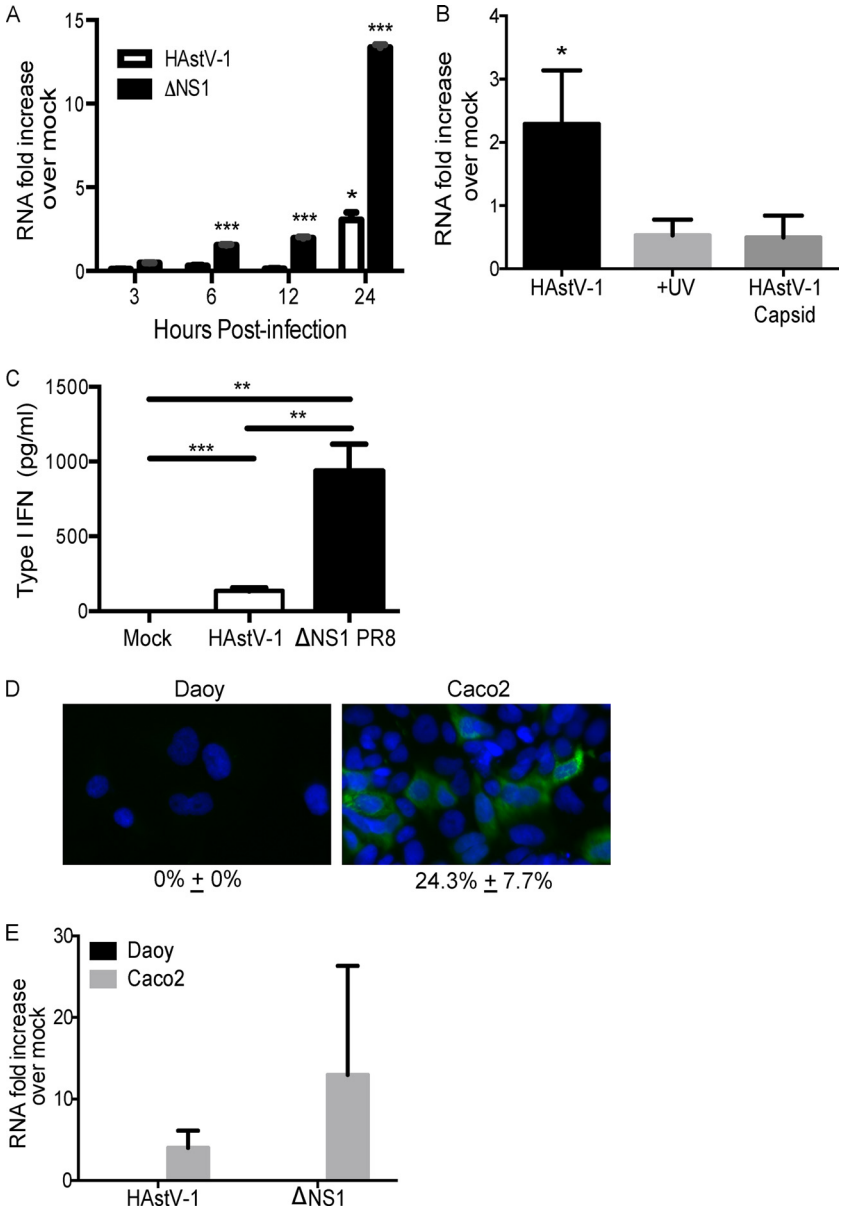

FIG 1 Type I IFN production is induced during HAstV-1 infection. (A) Differentiated Caco2 cells grown on transwell inserts were apically inoculated with PBS (mock infected), HAstV-1 (MOI of 1), or A/Puerto Rico/8/1934 influenza virus (PR8) lacking the NS1 gene (ΔNS1) (MOI of 0.3), and real-time RT-PCR for type 1 IFN (IFN-β) was performed on RNA normalized to GAPDH. Results are shown as fold increase over mock-infected cells at the same time point. (B) IFN-β RNA levels in Caco2 cells inoculated with HAstV-1, UV-inactivated HAstV-1 (MOI of 1), or 5 μg HAstV-1 capsid at 24 h postinoculation as described above for panel A. (C) Type I IFN levels were quantitated in supernatants at 24 hpi by bioassay on Daoy cells. (D) Daoy or Caco2 cells infected with HAstV-1 (MOI of 2) were stained for capsid 24 hpi. (E) IFN-β RNA levels of cells infected with HAstV-1 (MOI of 1) at 24 hpi as described above for panel A. Data are the average of two independent experiments performed at least three times (A to C) or twice (D and E). Error bars indicate standard deviations (SD). Asterisks show statistical significance as measured by the two-tailed Student *t* test as follows: *, $P < 0.05$; **, $P < 0.005$; ***, $P < 0.0005$.

netics of IFN-β induction during HAstV-1 infection, we next investigated whether HAstV-1 replication was sensitive to IFN-β. First, Caco2 cells received increasing doses of IFN-β for 18 h prior to and during the course of HAstV-1 infection (MOI of 1). Cells were then fixed at 24 hpi, and HAstV-1 levels were quantitated by the fluorescent-focus assay as described previously (24). Results are expressed as the percentage of cells expressing HAstV-1 capsid protein compared to the percentage of cells expressing HAstV-1 capsid protein in untreated HAstV-infected cells, which was set at 100%. Exogenous IFN-β decreased the percentage of cells with new HAstV-1 capsid synthesis in a dose-dependent manner (Fig. 2A) with 100 ng/ml resulting in a 90% reduction in capsid-expressing cells (Fig. 2B). Type 1 IFN bioassay results suggest that HAstV-1 infection results in ~0.1 ng/ml of active protein (Fig. 1C), suggesting that the type 1 IFN produced during infection could limit viral spread.

To test whether HAstV-1-induced IFN-β limits HAstV-1 replication during infection, Caco2 cells were infected with HAstV-1 (MOI of 1) in the presence of 3 μg/ml of a human IFN-β neutralizing antibody, an isotype IgG, or no antibody in medium con-

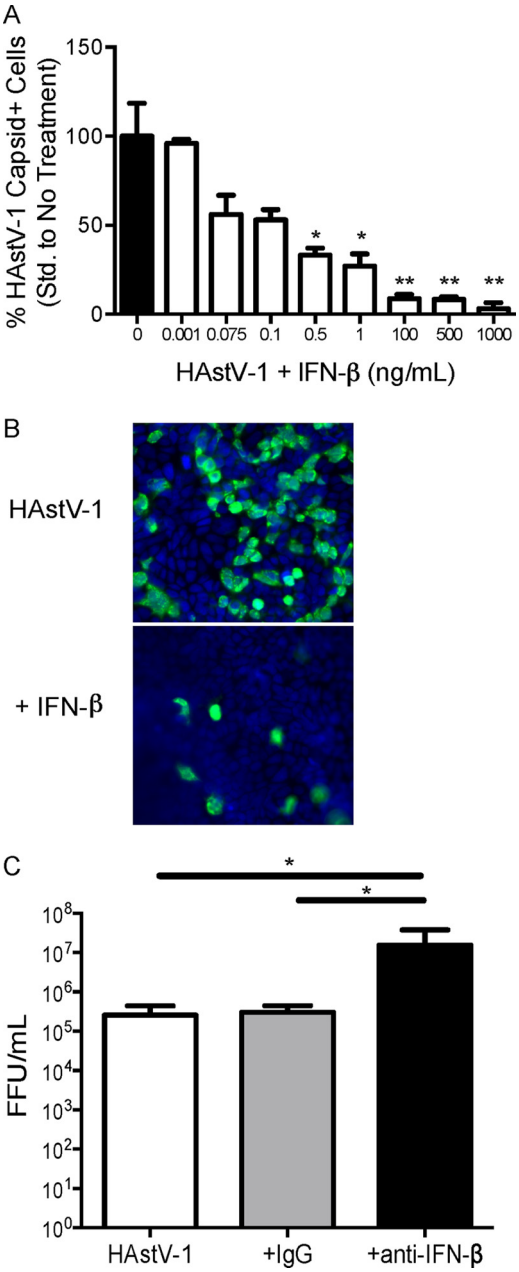

FIG 2 Type I IFN reduces HAstV-1 replication *in vitro*. (A) Differentiated Caco2 cells were treated with increasing concentrations of human IFN-β for 18 h prior to and during HAstV-1 infection (MOI of 1). Cells were fixed at 24 hpi and stained for HAstV-1 capsid by fluorescence microscopy. The number of positive cells per field with 10× lens objective was quantitated. Results are expressed as the percent capsid expression compared to untreated HAstV-infected cells (standardized [Std.] to no treatment), which was set at 100%. (B) Representative images of HAstV-1-infected cells pretreated with 100 ng/ml IFN-β (+ IFN-β) or not pretreated with IFN-β. (C) Caco2 cells were treated with PBS or with 3 μg/ml control IgG or IFN-β neutralizing antibody during HAstV-1 (MOI of 1) infection in the presence of trypsin. Fresh Caco2 cells were then inoculated with 10-fold dilutions of supernatants collected at 24 hpi, cells were stained for HAstV-1 capsid at 24 hpi, and viral replication was quantitated by determining the number of fluorescent focus-forming units (FFU) per milliliter. Data are the averages of two independent experiments performed at least twice (A and C). Panel B shows representative images from two independent experiments. Error bars indicate SD. Asterisks show statistical significance as measured by the two-tailed Student *t* test as follows: *, $P < 0.05$; **, $P < 0.005$.

taining 10 μg/ml porcine trypsin, which is required for multiround HAstV-1 replication (37). Supernatants were collected at 24 hpi, and viral titers were determined by the fluorescent-focus assay. Inhibiting the endogenous IFN-β produced during HAstV-1 led to ~2.5-log-unit-higher viral titers compared to untreated or control IgG-treated cells (Fig. 2C). These data demonstrate that the amount of IFN-β that HAstV-1 induced during infection is sufficient to limit viral replication and correlate with recent work by Guix et al. demonstrating that IFN-β pretreatment of Caco2 cells reduces HAstV-4 capsid protein synthesis (17).

Our studies demonstrate that IFN-β inhibits HAstV-1 capsid expression (Fig. 2B). Thus, to define the stage at which it inhibits viral replication, IFN-β-pretreated Caco2 cells were infected with HAstV-1 (MOI of 5), RNA was collected at 1, 4, 8, and 16 hpi, and negative- and positive-strand RNA synthesis was monitored by RT-PCR and quantified using ImageJ using β-actin levels to standardize as described previously (24, 25, 38). IFN-β pretreatment did not impact RNA levels at 1 and 4 hpi, suggesting that IFN-β pretreatment has no effect on HAstV-1 entry (Fig. 3). However, IFN-β pretreatment markedly reduced levels of positive-strand RNA synthesis beginning at 8 hpi compared to untreated controls (Fig. 3A and B). At 8 hpi, IFN-β pretreatment led to a 50% reduction in positive-strand RNA compared to the nonpretreated cells, and levels remained decreased at 16 hpi. In contrast, negative-strand HAstV-1 RNA levels were statistically unaffected by IFN-β pretreatment (Fig. 3C and D). Although we did observe a trend toward decreased negative-sense RNA levels at 8 hpi in certain experiments, it was not statistically significant ($P = 0.07$). These data demonstrate that IFN-β decreases HAstV-1 replication after viral entry and decreases the levels of positive-strand HAstV-1 RNA. While Guix et al. found that IFN-β decreases HAstV-4 new capsid protein synthesis and progeny virion release (17), our data further delineate at which step in the replication cycle IFN-β decreases HAstV replication.

IFN-β protects against HAstV-1-induced epithelial barrier permeability. Arguably, one of the most important roles of the intestinal epithelium is to provide a barrier to regulate the transport of solutes and pathogens into the body, and the flux of water outside the body, which can lead to diarrhea if dysregulated (39–42). It does so by forming regulated epithelial cell-cell associations known as tight junctions. Tight junctions are made up of transmembrane proteins that form homotypic and heterotypic interactions to form a dynamic barrier that is essentially impermeable to the movement of fluids and solutes between the luminal and serosal compartments (43). We demonstrated that HAstV-1 disrupts this epithelial permeability and tight junctions through an as yet undefined mechanism(s) (18). To determine whether IFN-β plays a role in HAstV-1-induced barrier permeability, we first measured TER of differentiated Caco2 cells pretreated with exogenous IFN-β and then infected with HAstV-1 (MOI of 2). As shown previously, HAstV-1 leads to a rapid decease in TER (Fig. 4A) (18). However, pretreatment with IFN-β significantly reduced the HAstV-1-induced decrease in TER at 24 to 36 hpi from a 60 to 80% reduction in TER (compared to time zero) to a 40% decrease (Fig. 4A).

To determine whether the drop in TER correlated with a change in permeability, we monitored the transmigration of 20-kDa FITC-labeled dextran from the apical chamber to the basolateral chamber during HAstV-1 infection (MOI of 2) of differentiated Caco2 cells in the presence or absence of IFN-β, a

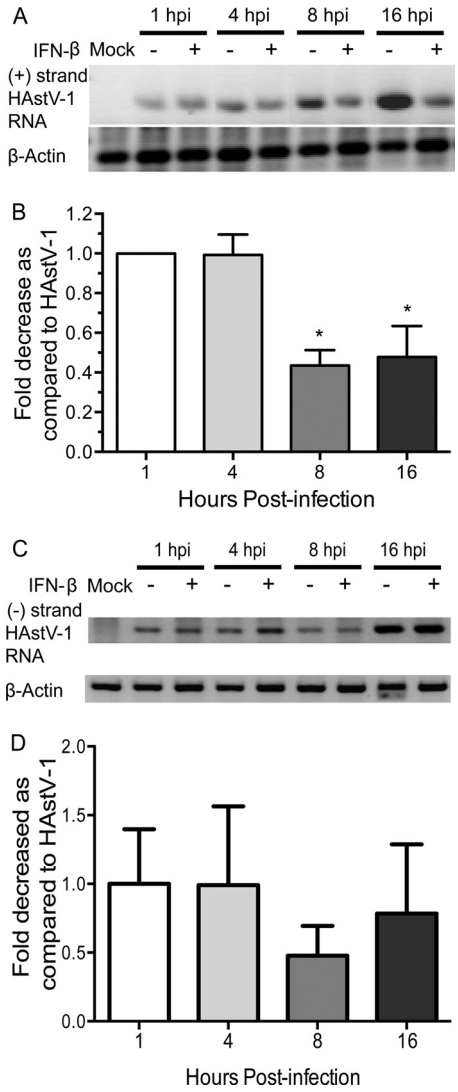

FIG 3 Positive-sense RNA synthesis is decreased by IFN-β pretreatment. Caco2 cells were mock infected or infected with HAstV-1 (MOI of 5) in the presence (+) or absence (−) of 1 μg/ml IFN-β, and RNA was collected at the times indicated above the lanes. RT-PCR using HAstV-specific Mon340/348 for the positive strand [(+) strand] (A and B), Mon343/344 for the negative strand [(−) strand] (C and D), or β-actin primers was performed on RNA (1 μg) followed by PCR with the corresponding primer pair as described in reference 24. The fold decrease in HAstV-1 RNA levels compared to untreated cells at the same time point was quantitated by ImageJ by standardizing to β-actin levels (B and D). Panel A shows a representative image from three independent experiments, while panel B shows the averages of three independent experiments. Panel C shows a representative image of two independent experiments, while panel D shows the averages of two independent experiments. Error bars indicate SD. *, $P < 0.05$ as measured by two-tailed Student *t* test to 1 hpi.

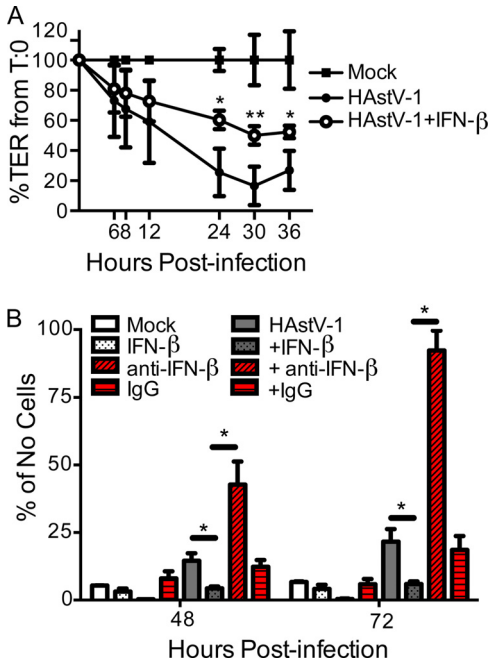

FIG 4 Type I IFN prevents barrier permeability of Caco2 cells during HAstV-1 infection. Differentiated Caco2 cells on transwell inserts were treated with 1 μg/ml of IFN-β or 3 μg/ml anti-IFN-β neutralizing antibody or control IgG for 18 h prior to inoculation with PBS (mock infected) or HAstV-1 (MOI of 2). (A) TER was measured at the indicated times and normalized to each sample's baseline at time zero. (B) Paracellular permeability was measured by the migration of 20-kDa FITC-labeled dextran to the basal chamber. Fluorescence was compared to that of the maximum migration of the probe across a cell-free insert; results are expressed as percentages of the maximum migration (percentage of no cell). Data are the averages from at least duplicate samples in two independent experiments. Error bars indicate SD. Asterisks show statistical significance as measured by the two-tailed Student *t* test as follows: *, $P < 0.05$; **, $P < 0.01$.

neutralizing antibody, or isotype control IgG. Results are expressed as the percentage of FITC migration across a cell-free insert (percentage of no cells) as described previously (18). FITC-dextran levels did not increase above the level for mock-infected cells at 24 hpi for any of our treatments. In contrast, at 48 hpi, HAstV-1 infection increased barrier permeability by 20% compared to mock-infected cells. The addition of exogenous IFN-β completely protected the cells, while the addition of an IFN-β neutralizing antibody resulted in a 5-fold increase in permeability compared to HAstV-1-infected cells. The isotype control IgG had no effect (Fig. 4B). These results were even more significant at 72 hpi. Overall, our results suggest that type I IFNs protect the epithelial barrier and prevent permeability during astrovirus infection.

Type I IFN signaling limits astrovirus replication and barrier permeability *in vivo*. Finally, to determine the importance of type 1 IFNs in astrovirus infection *in vivo*, we developed a novel murine astrovirus (MuAstV) model based on our and other groups' findings that many laboratory mice are endogenously infected with MuAstV (23, 44). To do this, we screened our St. Jude colonies for MuAstV by real-time PCR and found that numerous immunocompromised strains including CD1, RAG, and type 1 IFN-α receptor (IFNaR) knockout mice (as examples) were persistently shedding MuAstV. Sequence analysis on ~500 nucleotides of the ORF2 revealed that our colonies are infected with an MuAstV genotype most similar to STL4 (Fig. 5A) (23). The capsid is 99% similar to STL4 at the nucleotide level and 98% similar via amino acid. We prepared a fecal filtrate containing 2×10^7 genomic copies of MuAstV and orally gavaged MuAstV-negative 3- to 6-week-old WT C57BL/6 mice and MuAstV-positive IFNaR knockout mice ($>10^6$ copies/μg RNA). Stool samples were collected from individual mice −1 to 53 days postinfection (dpi) to

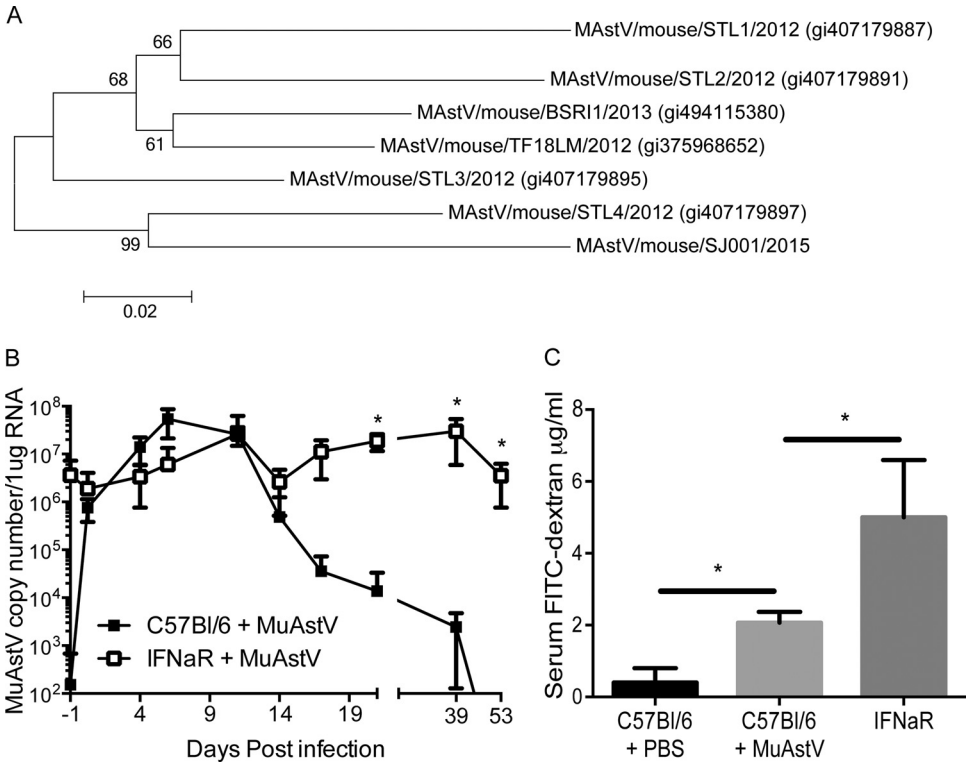

FIG 5 Type I IFN contributes to MuAstV control *in vivo*. (A) Phylogenetic tree of St. Jude MuAstV based on capsid sequence from residues 1267 to 1823 in ORF2. Alignment and tree generated in MEGA6 with the bootstrap values shown. The evolutionary history was inferred using the neighbor-joining method. The tree is drawn to scale, with branch lengths in the same units as those of the evolutionary distances used to infer the phylogenetic tree. The evolutionary distances were computed using the maximum composite likelihood method and are in the units of the number of base substitutions per site. (B) Three- to 6-week-old C57BL/6 or IFNaR$^{-/-}$ mice were orally gavaged with PBS or 2×10^7 genome copies of MuAstV, and viral shedding was monitored by real-time RT-PCR on fresh feces as the indicated times postinfection. (C) Four-kilodalton FITC-dextran was administered by oral gavage at 3 dpi, blood samples were collected 4 h after administration of FITC-dextran, and fluorescence intensity in the sera was measured. The concentration of FITC-dextran in sera was determined by comparison to a FITC-dextran standard curve. Data are the averages from two independent experiments performed at least twice Error bars indicate SD. Values that are statistically significantly different ($P < 0.05$) as measured by the two-tailed Student *t* test are indicated by an asterisk.

monitor viral replication or shed virus by real-time RT-PCR. WT mice began shedding virus within 2 dpi, and viral titers reached a peak of $>10^7$ copies/µg RNA between 6 and 11 dpi before decreasing over the remainder of the study, ultimately clearing by 53 dpi. In contrast, IFNaR$^{-/-}$ mice were shedding $>10^6$ copies/µg RNA in their feces at day −1, increasing slightly between days 9 and 14 postinfection, and continued shedding $>10^7$ copies/µg RNA throughout the experiment (Fig. 5B). These data strongly suggest that type I IFN is important for controlling astrovirus infection *in vivo*.

To monitor the impact on intestinal permeability, 4-kDa FITC-dextran (10 mg/100 g body weight) (Sigma) was orally administered to PBS-inoculated WT, MuAstV-infected WT and IFNaR$^{-/-}$ mice 3 dpi, blood samples were collected 4 h after administration, and fluorescence levels in sera were determined as described previously (32). WT mice inoculated with PBS had little FITC-dextran in their sera, whereas MuAstV-infected mice had significantly increased levels (0.4 µg/ml versus 2.1 µg/ml [Fig. 5C]). IFNaR$^{-/-}$ mice, which persistently shed MuAstV, had even higher levels of FITC-dextran in their sera than MuAstV-infected C57BL/6 mice did (2.1 µg/ml versus 5.0 µg/ml [Fig. 5C]), which correlates with our *in vitro* observations. Combined, our *in vivo* studies using an exciting new astrovirus animal model highlight the importance of type I IFN not only in controlling MuAstV infection but potentially in protecting the intestinal epithelial barrier from astrovirus-induced permeability, although we will need "clean" (MuAstV-free) IFNaR$^{-/-}$ mice to definitively delineate the role of type 1 IFN in intestinal permeability.

DISCUSSION

In this study, we demonstrate that HAstV-1 induces IFN-β production, which limits astrovirus replication *in vitro* and is important for the clearance of astrovirus *in vivo*. Our studies expand on the work of Guix et al. using HAstV-4, which determined that IFN-β induction occurs late in infection and is independent of replication (17). Here, we found that IFN-β reduces HAstV-1 replication in a dose-dependent manner and, importantly, that the amount of IFN-β produced during HAstV-1 infection is sufficient to limit replication, as treatment with an IFN-β neutralizing antibody increased HAstV-1 titers (Fig. 2C). We also further explored the step in the viral life cycle inhibited by IFN-β. Viral entry was not inhibited, since positive-strand HAstV-1 RNA levels were not significantly different between untreated and pretreated cells. However, at later times (8 and 16 hpi), positive-strand RNA levels were reduced in IFN-β-pretreated cells (Fig. 3A and B). We observed a trend toward reduced negative-strand HAstV-1 RNA levels at 8 hpi with IFN-β pretreatment, but it was not significant. IFN-β pretreatment could be inhibiting HAstV-1 positive-strand

production directly or at a step downstream of entry but upstream of positive-strand synthesis. Unfortunately, we were unable to measure the levels of nonstructural proteins due to the limited availability of characterized antibodies to these proteins. With the development of new tools, future studies can explore the mechanism(s) leading to inhibition of HAstV-1 replication by IFN-β *in vitro*.

In addition to inhibiting replication, we demonstrated that type I IFN may be important in protecting the epithelial barrier during HAstV infection. Pretreatment of Caco2 cells with exogenous IFN-β led to protection, while neutralizing endogenous levels led to a significant increase in permeability over infection alone. We know that binding of the capsid alone is sufficient to reduce TER (18), which quickly recovers once the capsid is removed. However, during a productive infection, we postulate that initial viral binding leads to a drop in TER within 12 to 16 hpi. At that time, progeny virus is released, leading to new capsid binding to surrounding cells in the monolayer. The production and release of IFN-β at 24 hpi (Fig. 1A) not only inhibit viral replication in surrounding cells but may also directly or indirectly protect the epithelium from virus-increased permeability. However, it is likely that the model is much more complicated given that exogenous IFN-β reduced the HAstV decrease in TER but did not completely abolish it (Fig. 4A), yet it did completely protect against the HAstV-increased fluorescent flux (Fig. 4B). Studies are ongoing to understand the cellular mechanism(s) of astrovirus-increased permeability.

The integrity of the barrier in our study differs from that of Guix et al., which concluded a positive correlation between IFN-β RNA production and barrier permeability (17). However, they directly tested the effect of IFN-β treatment on epithelial barrier permeability only in the absence of infection and found no difference in TER between IFN-β-treated cells and untreated cells (17). We found a direct effect of IFN-β on HAstV-1-induced barrier permeability in our differentiated Caco2 cells. Given that previous studies have demonstrated type I IFN′s stabilizing effect on endothelial cell monolayers by blocking IFN-γ-induced disintegration of tight junction complexes during the progression of multiple sclerosis, this further highlights the importance of the type I IFN system in protecting the host from increased barrier permeability during HAstV-1 infection (45, 46).

More importantly, we highlight the importance of type I IFN in astrovirus control and pathogenesis *in vivo* by characterizing a new mouse model of astrovirus infection. Previously, the only model for astrovirus pathogenesis was TAstV-2-infected turkey poults. Although this model has provided invaluable information, it is very limited in terms of accessibility, reagents, and genetics. In this work, we demonstrate that orally gavaging wild-type C57BL/6 mice with MuAstV-positive fecal filtrate results in productive infection, viral shedding, and increased intestinal permeability. Similar results were obtained using sucrose-purified MuAstV. Viral titers peaked at days 6 to 11 postinfection and then decreased, becoming negative at 53 dpi (Fig. 5B). In contrast, we found that our IFNaR$^{-/-}$ colony were endogenously infected with MuAstV and persistently shed virus. Whether the persistent infection is due to the inability to clear the initial infection or whether shedding is due to constant reinfection cannot be determined until we generate MuAstV-free IFNaR$^{-/-}$ mice. The IFNaR$^{-/-}$ mice also had increased intestinal permeability compared to MuAstV-infected WT mice, despite the fact that these mice had similar levels of MuAstV when administered FITC-dextran (Fig. 5C). Although higher levels of FITC-dextran in the sera of IFNaR$^{-/-}$ mice could be due to infection with MuAstV for a longer period of time than WT mice, these data correlate with our *in vitro* TER and fluorescence flux assays, which demonstrated that pretreatment of differentiated Caco2 cells with IFN-β protects against HAstV-1-induced barrier permeability and inhibiting the virus-induced type I IFN led to a significant increase in permeability (Fig. 4).

In conclusion, this work provides initial evidence that the type I IFN system can limit HAstV-1 replication both *in vitro* and *in vivo*. The use of mice as a small-animal model can be used to advance our understanding of astrovirus pathogenesis and infection. Furthermore, this study delineated type I IFN′s role in limiting permeability of epithelial cell monolayers induced by astrovirus infection *in vitro* and intestinal barrier permeability *in vivo*. An important next step will be generating MuAstV-free IFNaR$^{-/-}$ mice. All of the mice in our IFNaR$^{-/-}$ colony are MuAstV positive. This may have occurred through contact with infected animals or bedding, given that cohousing can lead to infection (23), as can exposure to contaminated bedding (B. Sharp et al., unpublished data). Regardless, generating MuAstV-free mice will be important not only to understand astrovirus pathogenesis and control but also to determine whether asymptomatic endogenous MuAstV infections influence the outcome of other scientific studies, such as infections with other agents, pharmaceutical treatments, or microbiome work. Like murine norovirus, it will also be important to explore the impact of diverse MuAstV strains on pathogenesis, systemic spread, and research with murine models.

ACKNOWLEDGMENTS

We thank Lee-Ann Van de Velde and the laboratory of Paul Thomas for providing reagents and Victoria Meliopoulos and Cydney Johnson for technical expertise.

FUNDING INFORMATION

ALSAC and The Hartwell Foundation provided funding to Stacey Schultz-Cherry.

REFERENCES

1. **Holloway G, Coulson BS.** 2013. Innate cellular responses to rotavirus infection. J Gen Virol **94:**1151–1160. http://dx.doi.org/10.1099/vir.0.051276-0.
2. **Feng Q, Hato SV, Langereis MA, Zoll J, Virgen-Slane R, Peisley A, Hur S, Semler BL, van Rij RP, van Kuppeveld FJ.** 2012. MDA5 detects the double-stranded RNA replicative form in picornavirus-infected cells. Cell Rep **2:**1187–1196. http://dx.doi.org/10.1016/j.celrep.2012.10.005.
3. **Sherwood V, King E, Totemeyer S, Connerton I, Mellits KH.** 2012. Interferon treatment suppresses enteric adenovirus infection in a model gastrointestinal cell-culture system. J Gen Virol **93:**618–623. http://dx.doi.org/10.1099/vir.0.037556-0.
4. **Frias AH, Jones RM, Fifadara NH, Vijay-Kumar M, Gewirtz AT.** 2012. Rotavirus-induced IFN-beta promotes anti-viral signaling and apoptosis that modulate viral replication in intestinal epithelial cells. Innate Immun **18:**294–306. http://dx.doi.org/10.1177/1753425911401930.
5. **Walter JE, Mitchell DK.** 2000. Role of astroviruses in childhood diarrhea. Curr Opin Pediatr **12:**275–279. http://dx.doi.org/10.1097/00008480-200006000-00018.
6. **Kurtz JB, Lee TW, Craig JW, Reed SE.** 1979. Astrovirus infection in volunteers. J Med Virol **3:**221–230. http://dx.doi.org/10.1002/jmv.1890030308.
7. **Glass RI, Noel J, Mitchell D, Herrmann JE, Blacklow NR, Pickering LK, Dennehy P, Ruiz-Palacios G, de Guerrero ML, Monroe SS.** 1996. The changing epidemiology of astrovirus-associated gastroenteritis: a review. Arch Virol Suppl **12:**287–300. http://dx.doi.org/10.1007/978-3-7091-6553-9_31.
8. **De Benedictis P, Schultz-Cherry S, Burnham A, Cattoli G.** 2011. Astro-

virus infections in humans and animals - molecular biology, genetic diversity, and interspecies transmissions. Infect Genet Evol **11:**1529–1544. http://dx.doi.org/10.1016/j.meegid.2011.07.024.
9. **Donelli G, Superti F, Tinari A, Marziano ML.** 1992. Mechanism of astrovirus entry into Graham 293 cells. J Med Virol **38:**271–277. http://dx.doi.org/10.1002/jmv.1890380408.
10. **Willcocks MM, Carter MJ.** 1993. Identification and sequence determination of the capsid protein gene of human astrovirus serotype 1. FEMS Microbiol Lett **114:**1–7. http://dx.doi.org/10.1111/j.1574-6968.1993.tb06542.x.
11. **Monroe SS, Jiang B, Stine SE, Koopmans M, Glass RI.** 1993. Subgenomic RNA sequence of human astrovirus supports classification of Astroviridae as a new family of RNA viruses. J Virol **67:**3611–3614.
12. **Jang SY, Jeong WH, Kim MS, Lee YM, Lee JI, Lee GC, Paik SY, Koh GP, Kim JM, Lee CH.** 2010. Detection of replicating negative-sense RNAs in CaCo-2 cells infected with human astrovirus. Arch Virol **155:**1383–1389. http://dx.doi.org/10.1007/s00705-010-0718-9.
13. **Mendez E, Aguirre-Crespo G, Zavala G, Arias CF.** 2007. Association of the astrovirus structural protein VP90 with membranes plays a role in virus morphogenesis. J Virol **81:**10649–10658. http://dx.doi.org/10.1128/JVI.00785-07.
14. **Guix S, Caballero S, Bosch A, Pinto RM.** 2004. C-terminal nsP1a protein of human astrovirus colocalizes with the endoplasmic reticulum and viral RNA. J Virol **78:**13627–13636. http://dx.doi.org/10.1128/JVI.78.24.13627-13636.2004.
15. **Gray EW, Angus KW, Snodgrass DR.** 1980. Ultrastructure of the small intestine in astrovirus-infected lambs. J Gen Virol **49:**71–82. http://dx.doi.org/10.1099/0022-1317-49-1-71.
16. **Mendez E, Salas-Ocampo E, Arias CF.** 2004. Caspases mediate processing of the capsid precursor and cell release of human astroviruses. J Virol **78:**8601–8608. http://dx.doi.org/10.1128/JVI.78.16.8601-8608.2004.
17. **Guix S, Perez-Bosque A, Miro L, Moreto M, Bosch A, Pinto RM.** 2015. Type I interferon response is delayed in human astrovirus infections. PLoS One **10:**e0123087. http://dx.doi.org/10.1371/journal.pone.0123087.
18. **Moser LA, Carter M, Schultz-Cherry S.** 2007. Astrovirus increases epithelial barrier permeability independently of viral replication. J Virol **81:**11937–11945. http://dx.doi.org/10.1128/JVI.00942-07.
19. **Koci MD, Moser LA, Kelley LA, Larsen D, Brown CC, Schultz-Cherry S.** 2003. Astrovirus induces diarrhea in the absence of inflammation and cell death. J Virol **77:**11798–11808. http://dx.doi.org/10.1128/JVI.77.21.11798-11808.2003.
20. **DuBois RM, Freiden P, Marvin S, Reddivari M, Heath RJ, White SW, Schultz-Cherry S.** 2013. Crystal structure of the avian astrovirus capsid spike. J Virol **87:**7853–7863. http://dx.doi.org/10.1128/JVI.03139-12.
21. **Hoffmann E, Krauss S, Perez D, Webby R, Webster RG.** 2002. Eight-plasmid system for rapid generation of influenza virus vaccines. Vaccine **20:**3165–3170. http://dx.doi.org/10.1016/S0264-410X(02)00268-2.
22. **Karlsson EA, Meliopoulos VA, Savage C, Livingston B, Mehle A, Schultz-Cherry S.** 2015. Visualizing real-time influenza virus infection, transmission and protection in ferrets. Nat Commun **6:**6378. http://dx.doi.org/10.1038/ncomms7378.
23. **Yokoyama CC, Loh J, Zhao G, Stappenbeck TS, Wang D, Huang HV, Virgin HW, Thackray LB.** 2012. Adaptive immunity restricts replication of novel murine astroviruses. J Virol **86:**12262–12270. http://dx.doi.org/10.1128/JVI.02018-12.
24. **Moser LA, Schultz-Cherry S.** 2008. Suppression of astrovirus replication by an ERK1/2 inhibitor. J Virol **82:**7475–7482. http://dx.doi.org/10.1128/JVI.02193-07.
25. **Belliot G, Laveran H, Monroe SS.** 1997. Detection and genetic differentiation of human astroviruses: phylogenetic grouping varies by coding region. Arch Virol **142:**1323–1334. http://dx.doi.org/10.1007/s007050050163.
26. **Meliopoulos VA, Kayali G, Burnham A, Oshansky CM, Thomas PG, Gray GC, Beck MA, Schultz-Cherry S.** 2014. Detection of antibodies against Turkey astrovirus in humans. PLoS One **9:**e96934. http://dx.doi.org/10.1371/journal.pone.0096934.
27. **Karlsson EA, Small CT, Freiden P, Feeroz MM, Matsen FA, IV, San S, Hasan MK, Wang D, Jones-Engel L, Schultz-Cherry S.** 2015. Non-human primates harbor diverse mammalian and avian astroviruses including those associated with human infections. PLoS Pathog **11:**e1005225. http://dx.doi.org/10.1371/journal.ppat.1005225.
28. **Kotla S, Peng T, Bumgarner RE, Gustin KE.** 2008. Attenuation of the type I interferon response in cells infected with human rhinovirus. Virology **374:**399–410. http://dx.doi.org/10.1016/j.virol.2008.01.022.
29. **Martinez-Sobrido L, Gitiban N, Fernandez-Sesma A, Cros J, Mertz SE, Jewell NA, Hammond S, Flano E, Durbin RK, Garcia-Sastre A, Durbin JE.** 2006. Protection against respiratory syncytial virus by a recombinant Newcastle disease virus vector. J Virol **80:**1130–1139. http://dx.doi.org/10.1128/JVI.80.3.1130-1139.2006.
30. **National Research Council.** 2011. Guide for the care and use of laboratory animals, 8th ed. National Academies Press, Washington, DC.
31. **Tang VW, Goodenough DA.** 2003. Paracellular ion channel at the tight junction. Biophys J **84:**1660–1673. http://dx.doi.org/10.1016/S0006-3495(03)74975-3.
32. **Calon A, Gross I, Lhermitte B, Martin E, Beck F, Duclos B, Kedinger M, Duluc I, Domon-Dell C, Freund JN.** 2007. Different effects of the Cdx1 and Cdx2 homeobox genes in a murine model of intestinal inflammation. Gut **56:**1688–1695. http://dx.doi.org/10.1136/gut.2007.125542.
33. **Wang X, Li M, Zheng H, Muster T, Palese P, Beg AA, Garcia-Sastre A.** 2000. Influenza A virus NS1 protein prevents activation of NF-kappaB and induction of alpha/beta interferon. J Virol **74:**11566–11573. http://dx.doi.org/10.1128/JVI.74.24.11566-11573.2000.
34. **Talon J, Horvath CM, Polley R, Basler CF, Muster T, Palese P, Garcia-Sastre A.** 2000. Activation of interferon regulatory factor 3 is inhibited by the influenza A virus NS1 protein. J Virol **74:**7989–7996. http://dx.doi.org/10.1128/JVI.74.17.7989-7996.2000.
35. **Guo Z, Chen LM, Zeng H, Gomez JA, Plowden J, Fujita T, Katz JM, Donis RO, Sambhara S.** 2007. NS1 protein of influenza A virus inhibits the function of intracytoplasmic pathogen sensor, RIG-I. Am J Respir Cell Mol Biol **36:**263–269. http://dx.doi.org/10.1165/rcmb.2006-0283RC.
36. **Geiss GK, Salvatore M, Tumpey TM, Carter VS, Wang X, Basler CF, Taubenberger JK, Bumgarner RE, Palese P, Katze MG, Garcia-Sastre A.** 2002. Cellular transcriptional profiling in influenza A virus-infected lung epithelial cells: the role of the nonstructural NS1 protein in the evasion of the host innate defense and its potential contribution to pandemic influenza. Proc Natl Acad Sci U S A **99:**10736–10741. http://dx.doi.org/10.1073/pnas.112338099.
37. **Bass DM, Qiu S.** 2000. Proteolytic processing of the astrovirus capsid. J Virol **74:**1810–1814. http://dx.doi.org/10.1128/JVI.74.4.1810-1814.2000.
38. **Rohayem J, Berger S, Juretzek T, Herchenroder O, Mogel M, Poppe M, Henker J, Rethwilm A.** 2004. A simple and rapid single-step multiplex RT-PCR to detect Norovirus, Astrovirus and Adenovirus in clinical stool samples. J Virol Methods **118:**49–59. http://dx.doi.org/10.1016/j.jviromet.2004.01.016.
39. **Madara JL.** 1998. Regulation of the movement of solutes across tight junctions. Annu Rev Physiol **60:**143–159. http://dx.doi.org/10.1146/annurev.physiol.60.1.143.
40. **Madara JL.** 1989. Loosening tight junctions. Lessons from the intestine. J Clin Invest **83:**1089–1094.
41. **Madara JL.** 1988. Tight junction dynamics: is paracellular transport regulated? Cell **53:**497–498. http://dx.doi.org/10.1016/0092-8674(88)90562-4.
42. **Madara JL.** 1987. Intestinal absorptive cell tight junctions are linked to cytoskeleton. Am J Physiol **253:**C171–C175.
43. **Balda MS, Matter K.** 2008. Tight junctions at a glance. J Cell Sci **121:**3677–3682. http://dx.doi.org/10.1242/jcs.023887.
44. **Farkas T, Fey B, Keller G, Martella V, Egyed L.** 2012. Molecular detection of novel astroviruses in wild and laboratory mice. Virus Genes **45:**518–525. http://dx.doi.org/10.1007/s11262-012-0803-0.
45. **Kraus J, Ling AK, Hamm S, Voigt K, Oschmann P, Engelhardt B.** 2004. Interferon-beta stabilizes barrier characteristics of brain endothelial cells in vitro. Ann Neurol **56:**192–205. http://dx.doi.org/10.1002/ana.20161.
46. **Minagar A, Long A, Ma T, Jackson TH, Kelley RE, Ostanin DV, Sasaki M, Warren AC, Jawahar A, Cappell B, Alexander JS.** 2003. Interferon (IFN)-beta 1a and IFN-beta 1b block IFN-gamma-induced disintegration of endothelial junction integrity and barrier. Endothelium **10:**299–307.